Histone H1 Dephosphorylation Is Not a General Feature in Early Apoptosis[†]

Anna Gréen,[‡] Bettina Sarg,[§] Elisavet Koutzamani,[‡] Ulrika Genheden,[‡] Herbert H. Lindner,*[,§] and Ingemar Rundquist*[,‡]

Division of Cell Biology, Department of Clinical and Experimental Medicine, Linköping University, SE-58185 Linköping, Sweden, and Division of Clinical Biochemistry, Biocenter, Innsbruck Medical University, Fritz-Pregl-Strasse 3, A-6020 Innsbruck, Austria

Received November 22, 2007; Revised Manuscript Received May 14, 2008

ABSTRACT: Histone H1 is a family of nucleosomal proteins that exist in a number of subtypes. These subtypes can be modified after translation in various ways, above all by phosphorylation. Increasing levels of H1 phosphorylation has been correlated with cell cycle progression, while both phosphorylation and dephosphorylation of histone H1 have been linked to the apoptotic process. Such conflicting results may depend on which various apoptosis-inducing agents cause apoptosis via different apoptotic pathways and often interfere with cell proliferation. Therefore, we investigated the relation between apoptosis and H1 phosphorylation in Jurkat cells after apoptosis induction via both the extrinsic and intrinsic pathways and by taking cell cycle effects into account. After apoptosis induction by anti-Fas, no significant dephosphorylation, as measured by capillary electrophoresis, or cell cycle-specific effects were detected. In contrast, H1 subtypes were rapidly dephosphorylated when apoptosis was induced by camptothecin. We conclude that histone H1 dephosphorylation is not connected to apoptosis in general but may be coupled to apoptosis by the intrinsic pathway or to concomitant growth inhibitory signaling.

DNA in the eukaryotic cell nuclei is compacted into chromatin by various proteins. The repeating unit of chromatin is the nucleosome. In the nucleosome core particle, 146 bp of DNA is wound around a protein octamer consisting of two copies of each core histone, H2A, H2B, H3, and H4. Histone H1 binds at (or near) the DNA entry−exit point on the nucleosome (*1*) and to the linker DNA, thereby stabilizing higher-order chromatin structure. The human histone H1 complement consists of at least nine subtypes, namely, H1.1−H1.5, H1°, H1t, H1.x, and oocyte-specific H1. The amount and composition of the H1 histones vary during embryonic development and cell differentiation (*2*). The role of H1 in chromatin has been debated. Most researchers agree that histone H1 stabilizes the nucleosome and higher-order chromatin structure, and that it is in some way involved in gene regulation.

The significance of having multiple subtypes remains unclear. Evolutionary data indicate that subtype differentiation is functional (*3*). However, several knockout experiments have demonstrated a remarkable redundancy of H1 subtypes, where the remaining subtypes seem to compensate for the loss of the others and maintain the H1-to-nucleosome ratio (*4*).

Histone H1 is also subject to various post-translational modifications. H1 phosphorylation may play a role in gene regulation, DNA repair, DNA replication, chromatin condensation, and apoptosis. H1 subtypes have been reported to incorporate phosphate groups during the cell cycle (*5*); recently, a number of H1 phosphorylation sites were mapped to serines in SP(K/A)K motifs in interphase chromatin, while during mitosis, H1.5 phosphorylation took place only at threonines (*6*). Histone H1 binding to chromatin is highly dynamic (*7*), and phosphorylation of H1 may cause an increased level of dissociation of H1 from chromatin (*8, 9*).

Apoptosis takes place in multicellular organisms during, for example, development, function of the immune system, maintenance of tissue homeostasis, and protection against DNA damage and cytotoxic agents (*10, 11*). Misregulation or nonfunctional apoptosis may cause, for instance, cancer, autoimmune disease, and neurodegenerative disease. Apoptosis is executed along two different pathways, the extrinsic pathway or the intrinsic (mitochondrial) pathway. The extrinsic pathway is triggered by activation of death receptors, like Fas (CD95) and tumor necrosis factor (TNF),[1] while the intrinsic pathway is activated by extra- or intracellular stress, for example, caused by DNA-damaging agents (*12*).

Histone H1 is believed to be involved in the apoptotic process in various ways. It is known to interact with and activate the major apoptotic nuclease, DFF40 (CAD in mice),

[†] This work, as part of European Science Foundation EUROCORES Programme EuroDYNA, was supported by funds from the Austrian Science Foundation (I23-B03) and the EC Sixth Framework Programme under Contract ERAS-CT-2003-980409.

* To whom correspondence should be addressed. I.R.: Department of Clinical and Experimental Medicine, Division of Cell Biology, Faculty of Health Sciences, Linköping University, SE-58185 Linköping, Sweden; phone, +46-13-224395; fax, +46-13-224314; e-mail, ingru@ibk.liu.se. H.H.L.: Division of Clinical Biochemistry, Biocenter, Innsbruck Medical University, Fritz-Pregl-Strasse 3, A-6020 Innsbruck, Austria; phone, +43-512-9003-70310; fax, +43-512-9003-70300; e-mail, herbert.lindner@i-med.ac.at.

[‡] Linköping University.

[§] Innsbruck Medical University.

[1] Abbreviations: TNF, tumor necrosis factor; Cam, camptothecin; 7-AAD, 7-aminoactinomycin D; PI, propidium iodide; PCA, perchloric acid; HPCE, high-performance capillary electrophoresis.

10.1021/bi702311x CCC: $40.75
Published on Web 06/18/2008

which cleaves the linker DNA between nucleosomes in chromatin during apoptosis (*13, 14*). H1.2 has been shown to play a direct role in the apoptotic signaling process following induction with X-ray irradiation or etoposide treatment, both of which give double-strand breaks, but not with other stimuli like TNF-α or UV irradiation. All H1 subtypes translocated to the cytoplasm after irradiation, but only H1.2 induced release of cytochrome *c* from mitochondria (*15*).

In response to low doses of ionizing radiation, dephosphorylation of H1 has been shown to occur (*16*). Dephosphorylation of some histone H1 subtypes during apoptosis has also been assumed to correlate with the initiation of apoptotic DNA fragmentation (*17*). In further experiments, this laboratory found that the dephosphorylation of H1 subtypes was an effect of alterations in cell cycle distribution promoted by topotecan instead of apoptosis (*18*) and that the state of H1 phosphorylation was not related to DNA fragmentation (*19*). H1 dephosphorylation was also reported in apoptotic NIH 3T3 cells (*20*). Other studies have reported increased levels of H1 phosphorylation following apoptosis induction in thymocytes with the phosphatase inhibitors calyculin A and okadaic acid; the increased level of phosphorylation was presumed to correlate with the triggering of DNA fragmentation (*21, 22*).

These conflicting data prompted us to investigate the H1 phosphorylation pattern in apoptotic Jurkat cells, taking cell cycle effects into account. Since histones, including H1, are released to the cytoplasm during the apoptotic process in Jurkat cells using anti-Fas or staurosporine and this release correlates in time with DNA fragmentation (*23*), we aimed to study H1 phosphorylation during early apoptosis. Apoptosis was induced via two different apoptotic pathways. Our results show that following Fas ligation, neither significant dephosphorylation of H1 subtypes nor any cell cycle alterations were detected, even though a large proportion of apoptotic cells were present. In contrast, histone H1 became rapidly dephosphorylated after camptothecin treatment, again without significant cell cycle alterations in the whole cell population, but selective apoptosis of G1 and S phase cells was confirmed. We conclude that histone H1 dephosphorylation is not connected to early apoptosis in general, but possibly to apoptosis via the intrinsic pathway or to affiliated growth inhibitory signaling.

EXPERIMENTAL PROCEDURES

Cell Culture. Jurkat cells (clone E6.1 from ECACC) were cultured at 37 °C with 5% CO_2 in RPMI 1640 supplemented with 10% (v/v) fetal bovine serum, penicillin (60 μg/mL), streptomycin (100 μg/mL), and L-glutamine (2 mM) (all Gibco, Paisley, Scotland, U.K.). The cells were subcultivated three times per week and kept at a density of $0.1-1 \times 10^6$ cells/mL. The day before apoptosis induction, the cells were seeded at a density of 0.25×10^6 cells/mL, to be in log growth phase with approximately 0.5×10^6 cells/mL for induction. The cell cultures were screened for mycoplasma and found to be negative.

Apoptosis Induction. Apoptosis was induced by adding either camptothecin (Cam, 5 μM, dissolved in DMSO) (Sigma, St. Louis, MO) or anti-Fas (25 ng/mL) (CH-11, Medical & Biological Laboratories, Nagoya, Japan) to the cell cultures. The cells were incubated for 2, 4, or 6 h at 37 °C with 5% CO_2. The cell concentration was determined prior to apoptosis induction and after incubation using a Z2 Coulter counter (Beckman Coulter, Fullerton, CA) or a Guava cell counter (Guava Technologies Inc., Hayward, CA).

Apoptosis Detection. Apoptosis was detected using annexin V-PE apoptosis detection kit I (BD Biosciences Pharmingen, San Diego, CA). Annexin V was conjugated with phycoerythrin (PE). To ensure measurement of early apoptosis, the cells were counterstained with 7-aminoactinomycin D (7-AAD) for detection of plasma membrane integrity. Annexin V-positive and 7-AAD-negative cells were considered early apoptotic cells. The cells were prepared according to the manufacturer's recommendations. Annexin-PE and 7-AAD fluorescence intensities were detected within 1 h using filter sets BP 575/26 and 670 LP at a BD LSR flow cytometer after excitation with an argon 488 nm laser. FSC and SSC were also detected; 15000 nongated events were collected. Compensation was set using single-stained samples. FSC and SSC were plotted; the cells were gated to exclude cell debris of low FSC and SSC, and fluorescence intensities for annexin-PE versus 7-AAD were plotted using BD CellQuest Pro (BD Biosciences). A quadrant marker was applied to discriminate nonapoptotic (PE-negative and 7-AAD-negative), apoptotic (PE-positive and 7-AAD-negative), late apoptotic/necrotic (PE-positive and 7-AAD-positive), and severely damaged cells (PE-negative and 7-AAD-positive). The two latter populations were added to give a late apoptotic/necrotic population.

The fraction of apoptotic cells with active caspases in the samples and the cell cycle status of the nonapoptotic and apoptotic populations were determined using the Vybrant FAM poly caspases assay kit (Molecular Probes, Eugene, OR). The Vybrant FAM poly caspases assay kit detects active caspases using a fluorescent inhibitor of caspases (FLICA), which attaches a fluoromethyl ketone (FMK) moiety with a carboxyfluorescein (FAM) reporter to a caspase-specific sequence, valine-alanine-aspartic acid (VAD). The reagent is cell-permeant and stains live cells. Unbound reagent is removed from the cell by washing. Detection of the remaining fluorescence gives the quantity of active caspases. To detect only intact cells, propidium iodide (PI) was used as a counterstain. FAM-positive and PI-negative cells are considered early apoptotic. For simultaneous measurement of the cell cycle distribution of apoptotic and nonapoptotic cells in the sample, Hoechst 33342 stain was added to samples during cell preparation.

To identify active caspases, samples were prepared according to the manufacturer's recommendations. After preparation, the samples were transferred to ice until they were analyzed using a BD LSR flow cytometer. Samples were excited using a 488 nm argon laser and a UV laser. PI, FAM, and Hoechst 33342 fluorescence were detected using filter sets LP 670, BP 530/28, and LP 380, respectively. Forward and side scatter were also obtained, and 30000 nongated particles were analyzed. Compensation was set between FAM and PI. Cells were gated by FSC and SSC to exclude cell debris of low FSC and SSC, and plots of FAM fluorescence against PI were obtained using CellQuest. Nonapoptotic (FAM-negative and PI-negative), apoptotic (FAM-positive and PI-negative), and late apoptotic/necrotic cell populations (PI-positive) were distinguished. The cell

cycle distribution of FAM-negative and PI-negative populations and FAM-positive and PI-negative populations was determined using ModFit LT (Verity Software House, Topsham, ME).

Cell Cycle Analysis. The cell cycle distribution of the total samples was determined using a method developed by Vindelöv (*24*). All chemicals were obtained from Sigma. Briefly, 10^6 cells were pelleted and resuspended in 50 μL of PBS; 180 μL of solution A (trypsin) was added, and the samples were incubated for 10 min and tubes inverted a few times. Then 180 μL of solution B (trypsin inhibitor and ribonuclease A) was added, and samples were incubated for an additional 10 min. This was performed at room temperature. Thereafter, 150 μL of solution C (propidium iodide and spermine tetrahydrochloride) was added, and the samples were placed on ice in the dark until they were analyzed. PI fluorescence was detected using a BP 575/26 filter on a BD LSR flow cytometer, as well as FSC and SSC. Fluorescence histograms of PI were analyzed using ModFit LT after gating cell nuclei by FSC and SSC to exclude debris of low FSC and SSC.

Extraction of H1 Histones. H1 histones were extracted with perchloric acid (PCA) from whole cells as described previously (*25*) with some minor changes. In control experiments, H1 extraction was performed from isolated nuclei as well as whole cells. All chemicals were obtained from Sigma unless otherwise indicated. All centrifugation steps were performed at 4 °C, and the samples were kept on ice. To all buffers and PCA were added 4-(2-aminoethyl)benzenesulfonyl fluoride hydrochloride (AEBSF), β-mercaptoethanol, and $Na_2S_2O_5$ (Merck, Darmstadt, Germany) to final concentrations of 1, 10, and 50 mM, respectively. All tubes and tips were siliconized. Briefly, approximately 75×10^6 Jurkat cells were harvested by centrifugation at 300*g* for 10 min. The cells were resuspended in STKM buffer [250 mM sucrose, 50 mM Tris-HCl (pH 7.5), 25 mM KCl, and 5 mM $MgCl_2 \cdot 6H_2O$ (Merck)] and centrifuged as described above. The cell pellet was resuspended in 1 mL of STKM buffer with 0.2% Triton X-100 (Merck), vortexed, and incubated for 10 min on ice. Nuclei were collected by centrifugation at 1500*g* for 10 min and washed once again with STKM without Triton. The permeabilization steps were omitted when H1 was extracted from whole cells.

Cell pellets containing nuclei or whole cells were extracted with 4 volumes of 5% PCA for 1 h on ice with occasional vortexing. After extraction, the samples were centrifuged for 10 min at 10000*g*, and the supernatant was moved to a new tube where 100% TCA was added to give a final concentration of 20%. The samples were vortexed; 300 μg of protamine sulfate was added, and samples were vortexed again and left at 4 °C overnight. Then the samples were centrifuged at 10000*g* for 10 min, and the supernatant was removed. The samples were washed once with acetone (Merck) and 1% HCl, centrifuged at 10000*g* for 10 min, and then washed in pure acetone and centrifuged as described above. The samples were dissolved in water with 0.01 M β-mercaptoethanol and centrifuged for 7 min at 6000*g*. The supernatant was moved to a new tube and lyophilized using a Speed-Vac (Heraeus Christ RVC 2-25, Heraeus-Christ, Osterode am Harz, Germany). Samples were kept at −20 °C until they were analyzed.

Capillary Electrophoresis. High-performance capillary electrophoresis (HPCE) was performed on a Beckman P/ACE 2100 system. Data collection and postrun data analyses were performed using P/ACE and System Gold software (Beckman Instruments). The capillary cartridge used was fitted with 75 μm internal diameter fused silica with a total length of 67 cm (60 cm to the detector). An untreated capillary was used in all experiments. Protein samples were injected by pressure, and detection was performed by measuring UV absorption at 200 nm. Separation of H1 histones was performed as described previously (*26, 27*). All runs were performed at a constant voltage (12 kV) and at a capillary temperature of 25 °C.

RESULTS

Exponentially growing Jurkat cells were treated with anti-Fas or Cam for 2, 4, or 6 h. For each sample, three sets of measurements were performed: (1) cell cycle distribution of the whole cell population, (2) apoptosis by annexin-V, and (3) apoptosis simultaneously with cell cycle distribution using the active caspase assay. Furthermore, histone H1 was extracted by PCA either from whole cells or from nuclei and separated by HPCE. Each set of experiments was repeated at least three times. The cell concentration of all samples was determined before apoptosis induction and at the times indicated for analysis. For all samples, it was found to be equal to or slightly higher after incubation with apoptosis inducers than before apoptosis induction (data not shown).

The apoptotic response of the samples was measured using annexin V, and the mean fractions of the nonapoptotic, apoptotic, and late apoptotic/necrotic populations were determined. Representative fluorescence plots from control, anti-Fas 6 h, and Cam 6 h are shown in Figure 1. The average proportions of the various populations are presented in Table 1, and the time course of the apoptotic response is illustrated in Figure 2A. For both inducers, the magnitude of the apoptotic response increased with time to 40% (anti-Fas) and 53.5% (Cam), while the level of late apoptotic/necrotic cells remained low (<12%) for both substances.

The apoptotic response was also determined by the active caspase assay. Simultaneously, cell cycle distributions of the nonapoptotic and apoptotic populations were analyzed using Hoechst 33342 staining. Typical fluorescence plots of control, anti-Fas 6 h, and Cam 6 h are presented in Figure 3 (top part) with discrimination of the nonapoptotic (R1, FAM-negative and PI-negative), apoptotic (R2, FAM-positive and PI-negative), and late apoptotic/necrotic (R3, PI-positive) cell populations. Statistics for the three gated regions (R1, R2, and R3) were calculated. Mean fractions of these populations are presented in Table 2, and progression of the apoptotic response over time is demonstrated in Figure 2B. The fraction of apoptotic cells after anti-Fas treatment was high (50.6%) already after 2 h but decreased slightly over time, while Cam treatment produced a rather weak apoptotic response (19.4% after 2 h), remaining at this level for 4 and 6 h. The level of late apoptotic/necrotic cells was low in the control sample (3.4%) but rapidly increased to 41.3% (anti-Fas 6 h) and 46% (Cam 6 h) during incubation with the two substances (Figure 2B).

Hoechst 33342 fluorescence histograms were obtained for the nonapoptotic and apoptotic populations and are illustrated

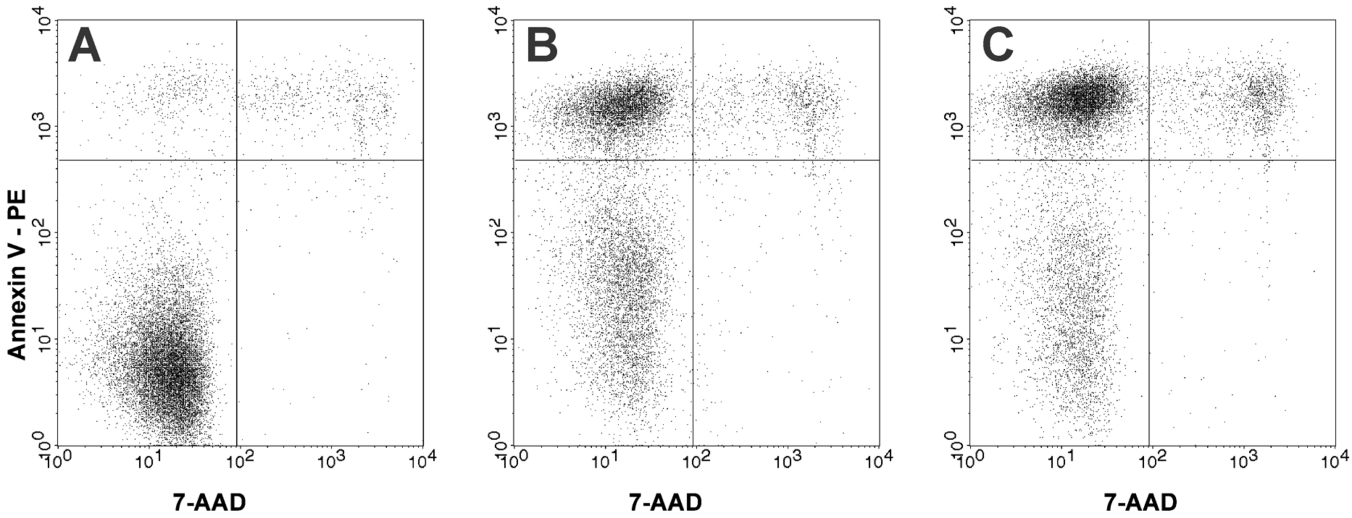

FIGURE 1: Annexin V analysis of Jurkat cells: bottom left quadrant, nonapoptotic cell population (PE-negative and 7-AAD-negative); top left quadrant, apoptotic cell population (PE-positive and 7-AAD-negative); and right quadrants, late apoptotic/necrotic cell populations (7-AAD-positive). (A) Control cells. (B) Anti-Fas 6 h. (C) Cam 6 h.

Table 1: Annexin-V Analysis of Jurkat Cell Samples after Apoptosis Induction (mean ± standard deviation; $n = 3$)[a]

sample	nonapoptotic (%)	apoptotic (%)	late apoptotic/ necrotic (%)
control	92.7 ± 1.3	1.7 ± 1.3	5.6 ± 0.3
anti-Fas 2 h	75.7 ± 2.3	17.6 ± 1.6	6.7 ± 2.4
anti-Fas 4 h	59.2 ± 6.9	31.6 ± 4.9	9.2 ± 2.0
anti-Fas 6 h	48.5 ± 6.3	40.0 ± 6.5	11.5 ± 0.1
Cam 2 h	85.3 ± 1.3	8.1 ± 1.4	6.6 ± 1.0
Cam 4 h	49.2 ± 4.9	42.7 ± 3.5	8.1 ± 1.3
Cam 6 h	35.4 ± 9.4	53.5 ± 7.9	11.1 ± 2.8

[a] The nonapoptotic population is annexin-PE-negative and 7-AAD-negative; the apoptotic population is annexin-PE-positive and 7-AAD-negative, and the late apoptotic/necrotic population is 7-AAD-positive.

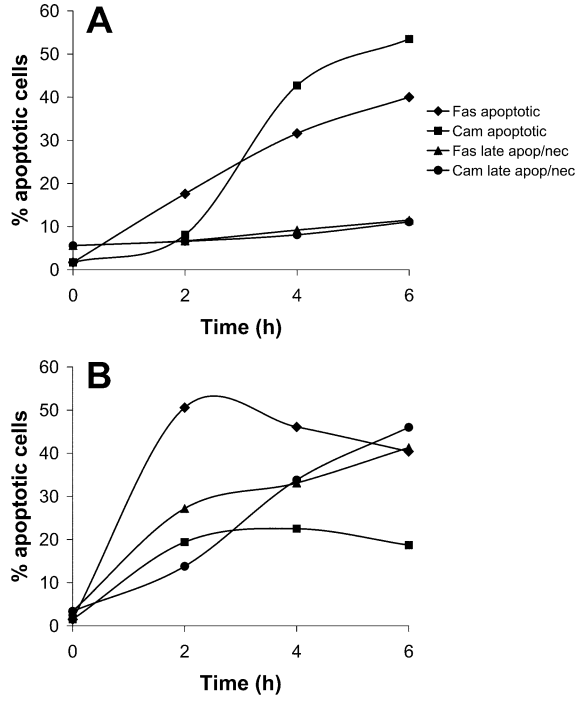

FIGURE 2: Time course of apoptotic response measured by (A) annexin and (B) the active caspase assay.

by the control and 6 h samples in Figure 3 (bottom part). Cell cycle distribution was analyzed using ModFit LT (data not shown).

After being treated with Cam for 2 h, the apoptotic cell population [19.4% (Table 2)] exhibited a very high proportion of both G1 and S phase cells (Figure 4B), while the nonapoptotic population exhibited a decrease in the level of S phase cells (Figure 4A) compared to the control (Figure 3A1). After being treated with Cam for 4 h, the apoptotic cells were primarily in the G1 phase, but still with a large fraction of S phase cells (Figure 4D), while the nonapoptotic population showed a substantially reduced level of S phase cells (Figure 4C) compared to the control (Figure 3A1). After the cells had been treated with Cam for 6 h, most of the apoptotic cells were in the G1 phase (Figure 3C2). Compared to 2 or 4 h of Cam treatment, a further reduction in the S phase fraction was seen (Figure 3C2), while the nonapoptotic population was nearly devoid of S phase cells (Figure 3C1), indicating that apoptosis was selectively induced by Cam in late G1 and early S phase cells.

The cell cycle phase distribution of the whole population of Cam-treated samples remained approximately the same as the control. Representative DNA histograms of control and 6 h samples are shown in panels A and C of Figure 5, respectively.

After apoptosis induction by anti-Fas, the cell cycle distributions of the apoptotic and nonapoptotic cell populations remained virtually unchanged. As illustrated by the 6 h sample, no major difference was seen between nonapoptotic (Figure 3B1) and apoptotic cells (Figure 3B2), and both populations also exhibited approximately the same cell cycle distribution as the control cells (Figure 3A1). Furthermore, PI staining of the total populations of anti-Fas-treated samples revealed no significant alterations in cell cycle distribution, as illustrated by the 6 h sample in Figure 5B, compared with the control (Figure 5A). These results demonstrate that apoptosis occurred in all cell cycle phases.

The number of cell nuclei exhibiting sub-G1 fluorescence was low after anti-Fas (Figure 5B) and Cam treatment (Figure 5C). These results indicate that only low levels of fragmented DNA were present in the apoptotic samples. This conclusion was further confirmed by DNA laddering experiments showing only tendencies for a DNA smear at 4 h and internucleosomal cleavage at 6 h (data not shown).

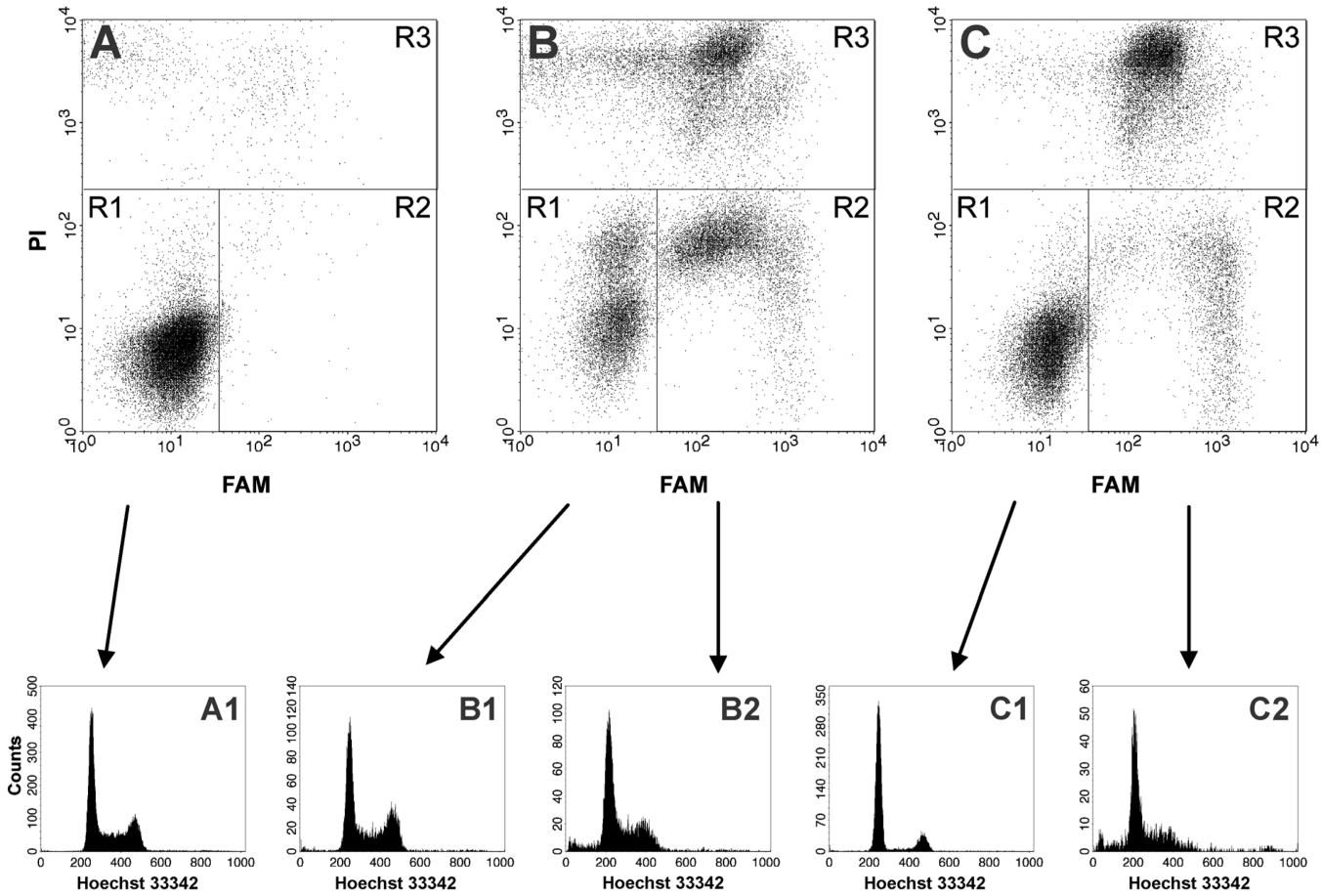

FIGURE 3: Detection of active caspases and cell cycle analysis of nonapoptotic and apoptotic cell populations: (A) control cells, (B) anti-Fas 6 h, and (C) Cam 6 h. Gate R1, nonapoptotic cell population (FAM- and PI-negative); gate R2, apoptotic cell population (FAM-positive and PI-negative); and gate R3, late apoptotic/necrotic cell population (PI-positive). Panels A1, B1, and C1 are cell cycle analyses using Hoechst 33342 of nonapoptotic populations. Panels B2 and C2 are cell cycle analyses using Hoechst 33342 of apoptotic populations.

Table 2: Apoptosis Analysis by Active Caspase Assay (mean ± standard deviation; $n = 3$)[a]

sample	nonapoptotic (%)	apoptotic (%)	late apoptotic/ necrotic (%)
control	95.1 ± 1.6	1.5 ± 1.0	3.4 ± 0.9
anti-Fas 2 h	22.2 ± 9.2	50.6 ± 12.0	27.2 ± 2.8
anti-Fas 4 h	20.8 ± 17.4	46.1 ± 16.5	33.1 ± 1.1
anti-Fas 6 h	18.3 ± 11.6	40.4 ± 10.7	41.3 ± 1.9
Cam 2 h	66.8 ± 3.4	19.4 ± 3.9	13.8 ± 0.6
Cam 4 h	43.7 ± 7.3	22.5 ± 9.2	33.8 ± 1.9
Cam 6 h	35.3 ± 9.3	18.7 ± 6.8	46.0 ± 2.8

[a] The nonapoptotic population is FAM-negative and PI-negative; the apoptotic population is FAM-positive and PI-negative, and the late apoptotic/necrotic population is PI-positive.

PCA-extracted histone H1 from exponentially growing control cells was analyzed by HPCE (Figure 6A). To prove the designation of individual unphosphorylated and phosphorylated H1 variants, H1 histones were first separated by RP-HPLC into two fractions, one containing H1.5 and one containing the remaining subtypes, H1.2−H1.4, as described previously (*6*). The first fraction was then reanalyzed by HPCE which allowed a clear assignment of unphosphorylated H1.5 and its phosphorylated forms, i.e., H1.5p0, H1.5p1, H1.5p2, and H1.5p3 (Supporting Information, Figure S1), in accordance with previous results (*6*). The second RP-HPLC fraction was further subjected to hydrophilic interaction liquid chromatography separation as described previously (*6*), resulting in six fractions containing H1.2p0,

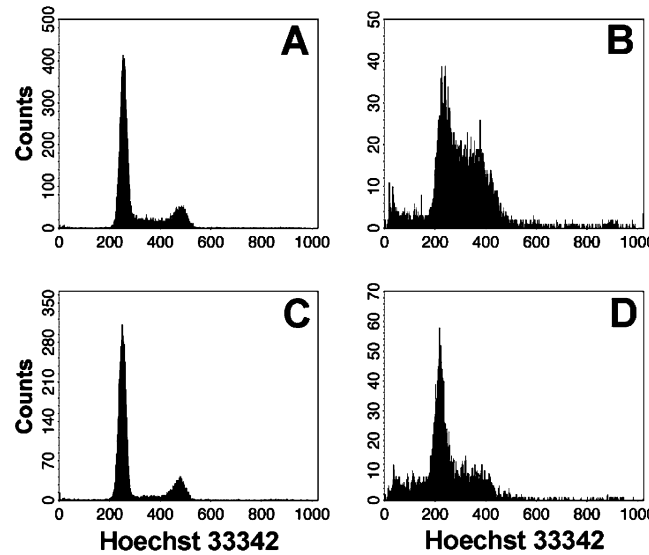

FIGURE 4: Hoechst 33342 histograms of nonapoptotic and apoptotic populations of camptothecin-treated cells: (A) Cam 2 h and nonapoptotic population, (B) Cam 2 h and apoptotic population, (C) Cam 4 h and nonapoptotic population, and (D) Cam 4 h and apoptotic population.

H1.3p0, H1.2p1, H1.4p0, H1.4p1, and H1.4p2 which were identified by mass spectrometry (unpublished data). These fractions were then used in mixing experiments (Supporting Information, Figure S2) to identify the peaks appearing in Figure 6. The migration order coincides exactly with recently

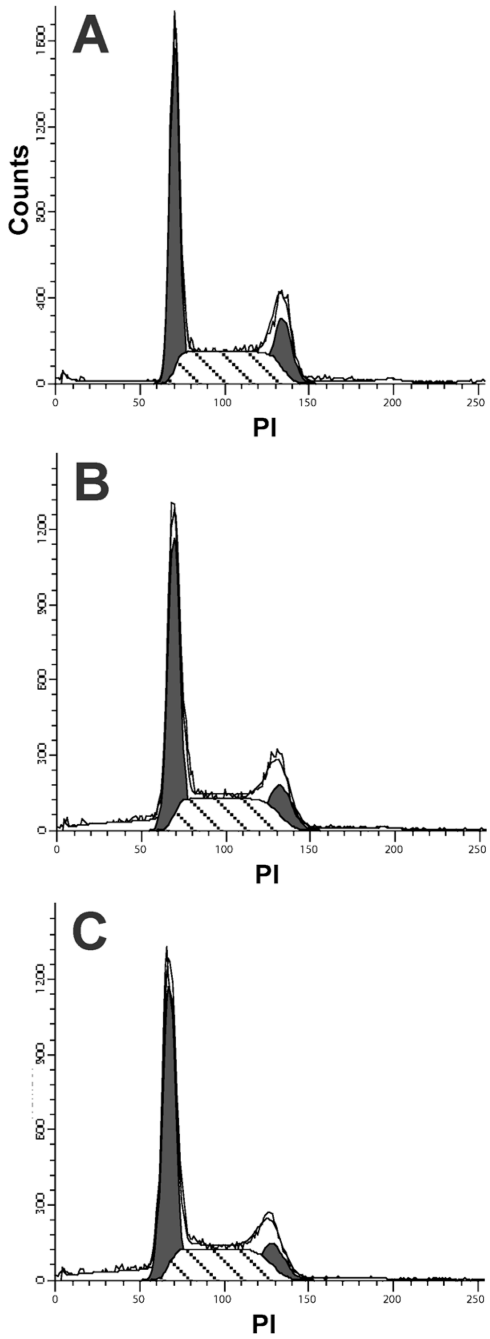

FIGURE 5: Cell cycle analyses of entire cell populations: (A) control cells, (B) anti-Fas 6 h, and (C) Cam 6 h.

published results (*19, 28*) obtained using the HPCE procedure developed in our laboratory.

Camptothecin treatment resulted in a major dephosphorylation of H1 subtypes after 2 h (Figure 6E) compared to the control (Figure 6A). The most prominent changes after Cam treatment were a clear increase in the level of unphosphorylated H1.5 (peak 1) and H1.4 (peak 2) subtypes and a decrease in the level of monophosphorylated H1.2 together with triphosphorylated H1.5 (peak 8) (Table 3). This dephosphorylation became even more evident after 4 (Figure 6F) and 6 h (Figure 6G). Since the number of nonapoptotic cells remained relatively high during Cam treatment (Tables 1 and 2), our results indicate that dephosphorylation was almost complete in the apoptotic cells or that dephosphorylation started before the appearance of the apoptotic markers. The corresponding phosphorylation pattern of H1 subtypes in the anti-Fas-treated samples (Figure 6B−D) remained approximately unchanged compared to that of the control (Figure 6A). After 6 h, a slight increase in the level of unphosphorylated H1.5 was observed (Figure 6D).

DISCUSSION

Histone H1 has previously been shown to be involved in apoptosis in various ways, but conflicting data have been obtained on the histone H1 phosphorylation pattern in apoptotic cells (*17–20, 22*). In this study, apoptosis was induced in Jurkat cells using anti-Fas and camptothecin that induce apoptosis along the two well-characterized pathways, the receptor-mediated, extrinsic pathway and the intrinsic pathway, respectively, to determine any differences in the H1 phosphorylation pattern between these pathways. We hypothesized that cell cycle effects may have affected previous studies of H1 phosphorylation and its connection to apoptosis, and we therefore combined apoptosis measurements with cell cycle analyses.

To ensure that cytoplasmic H1 did not escape our attention, we extracted H1 from whole cells as well as from isolated nuclei and analyzed the H1 subtypes and their phosphorylated forms by HPCE. No differences were detected between these samples, indicating that no selective loss of H1 variants occurred (data not shown). We also managed to obtain a high degree of apoptosis (up to 53.5%) within 6 h, without cellular DNA being highly fragmented and without extensive alterations in cellular size and membrane integrity.

Different apoptotic pathways are known to activate certain caspases at different times, while activation of others is a general feature of the apoptotic process. The number of different caspases that becomes activated and their level of activation is probably higher after anti-Fas apoptosis induction than after Cam induction (Figure 2B). Phosphatidylserine externalization is generally a later event than pan-caspase inhibitor binding (*29*). This is also illustrated by our results after apoptosis induction by anti-Fas, where a large fraction of cells with activated caspases (Figure 2B) preceded the maximum annexin response (Figure 2A). However, both inducers caused a substantial increase in the proportion of late apoptotic/necrotic cells as measured by the active caspase assay (Figure 2B) compared with annexin (Figure 2A). This can be explained by the addition of Hoechst 33342, which most likely enhanced the apoptotic effect of the inducers.

After apoptosis induction with anti-Fas, we detected only minor changes in the H1 phosphorylation pattern, indicating that the H1 subtypes in apoptotic Jurkat cells remained highly phosphorylated (Figure 6B−D). A small increase in the level of unphosphorylated H1.5 (Figure 6D and Table 3) was observed, suggesting that some initial H1 dephosphorylation may occur at this point. However, since the full H1 subtype phosphorylation pattern cannot be extracted quantitatively, this is not enough evidence to conclude that a biologically significant general H1 dephosphorylation occurred after anti-Fas treatment for 6 h, although it cannot be completely ruled out. Such an initial H1 dephosphorylation, maybe only of certain H1 subtype phosphorylation sites, is not unexpected and may be related to early events in growth inhibitory signaling. Furthermore, no or only minor changes were detected in the cell cycle distribution of Jurkat cells following induction of apoptosis by anti-Fas (Figure 5B). While this

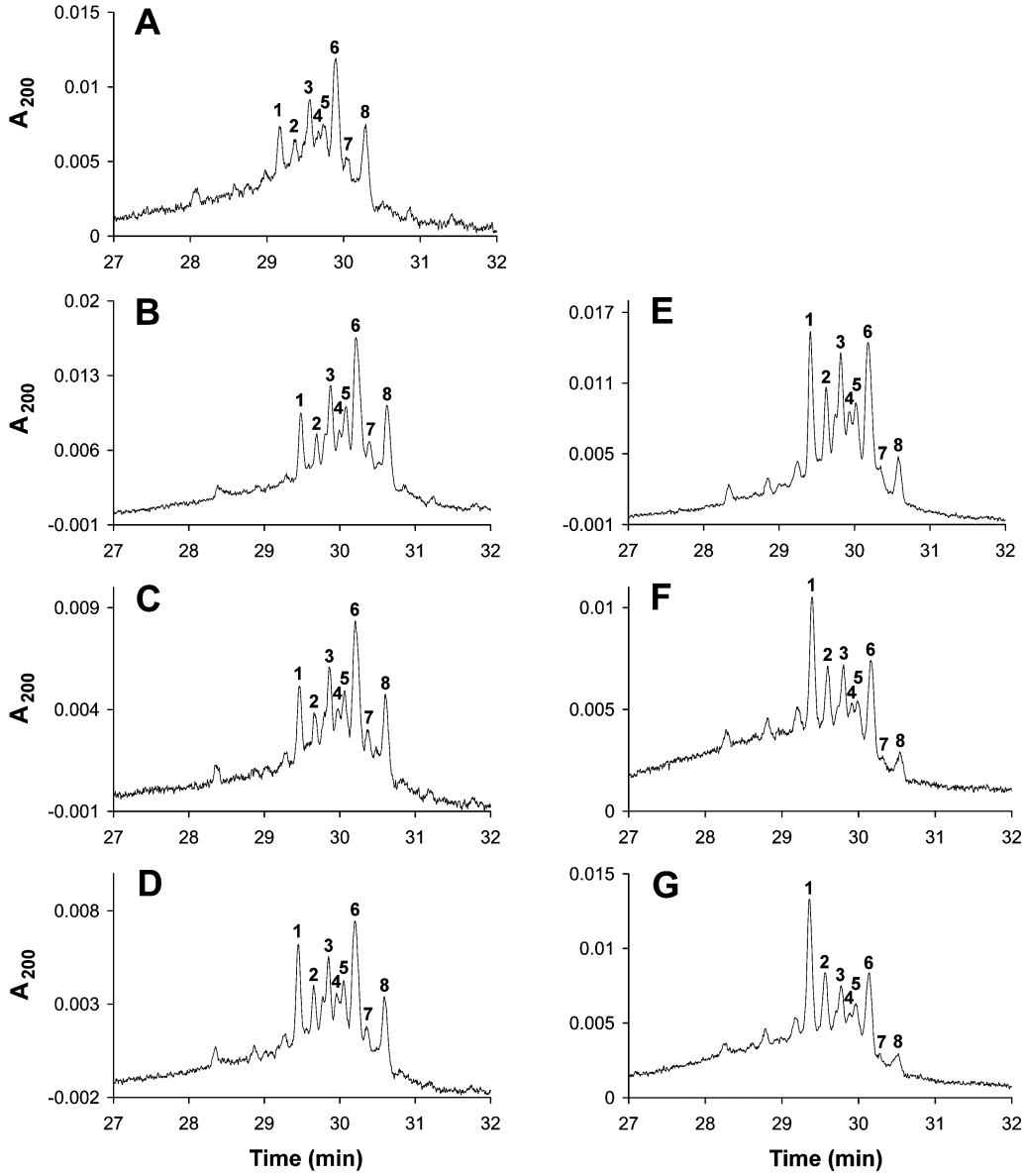

FIGURE 6: HPCE separations of perchloric acid-extracted H1 from Jurkat cells (whole cells): (A) exponentially growing control cells, (B) anti-Fas 2 h, (C) anti-Fas 4 h, (D) anti-Fas 6 h, (E) Cam 2 h, (F) Cam 4 h, and (G) Cam 6 h. The peak designations are unphosphorylated H1.5 (1), unphosphorylated H1.4 (2), monophosphorylated H1.5 (3), monophosphorylated H1.4 (4), unphosphorylated H1.3 (5), diphosphorylated H1.5 together with unphosphorylated H1.2, and possibly also diphosphorylated H1.4 (6), monophosphorylated H1.3 (7), and monophosphorylated H1.2 together with triphosphorylated H1.5 (8).

Table 3: Experimental Variations of HPCE Peak Heights (mean ± standard deviation) Measured as a Percentage of the Sum of all Eight Peak Heights

sample	peak 1 (%)	peak 2 (%)	peak 8 (%)	*n*
control	14.9 ± 1.0	6.1 ± 0.8	20.0 ± 1.4	4
anti-Fas 2 h	15.0 ± 1.9	6.3 ± 1.1	19.4 ± 1.0	4
anti-Fas 4 h	15.3 ± 1.5	7.4 ± 0.5	18.2 ± 1.5	4
anti-Fas 6 h	21.0 ± 0.6	8.3 ± 1.8	16.7 ± 1.8	3
Cam 2 h	29.0 ± 2.4	13.8 ± 0.6	8.0 ± 0.3	3
Cam 4 h	34.5 ± 1.2	15.2 ± 0.6	5.9 ± 0.4	3
Cam 6 h	37.2 ± 1.0	16.8 ± 1.6	5.0 ± 0.2	3

agrees with some previous observations (*30, 31*), other studies have indicated S phase arrest (*32*), apoptosis during the G1−S transition (*33*), or surviving cells preferentially being in the S+G2/M phase (*34*) following anti-Fas treatment of Jurkat cells. One study concluded that at low anti-Fas concentrations G0/G1 phase cells have a greater tendency to go into apoptosis, while at higher anti-Fas concentrations, no cell cycle preferences could be detected (*35*). However, these differences may be due to the use of different strains of Jurkat cells, different anti-Fas antibodies or other Fas ligands, and various concentrations of cells and antibodies and/or ligands. Variations in induction times and the use of different agents that can cause cell cycle alterations may also affect the results. In our study, we used a reasonably low anti-Fas concentration that still resulted in a strong apoptotic response in a short time, during which the cells were relatively undamaged. To the best of our knowledge, this is the first observation of a preserved H1 phosphorylation pattern during early apoptosis.

We also show that camptothecin-induced apoptosis of Jurkat cells prompted dephosphorylation of histone H1 after 2 h, accompanied by apoptosis of primarily G1 and S phase cells. No loss of cells was detected within 6 h of camptothecin-induced apoptosis. The cell cycle distribution of the whole samples was not affected, and only minor DNA

fragmentation was observed, which was probably due to the short incubation time. Camptothecin is a topoisomerase I inhibitor which binds to the DNA−topoisomerase complex, thereby causing DNA single-strand breaks. These are converted to double-strand breaks upon DNA replication, leading to S-phase-specific apoptosis mediated by caspases (*36, 37*), and camptothecin has previously been shown to induce apoptosis in G1/S Jurkat cells (*38*). Furthermore, Kratzmeier et al. (*17*) found that apoptosis in HL60 cells by topotecan treatment caused rapid H1 dephosphorylation. However, the H1 dephosphorylation in their system was later concluded to result from cell cycle effects caused by the topoisomerase I inhibitor topotecan, which promoted S phase selective apoptosis and selective loss of S and G2/M phase cells (*18*). Moreover, when using topotecan and Jurkat cells, a major decrease in the number of G2/M cells was found, but only a small change in the proportion of S phase cells, and this was accompanied by slower progression of dephosphorylation of H1 histones than for the HL60 system (*18*). In contrast, when using Jurkat cells and camptothecin, we observed a rapid dephosphorylation of H1 histones, which was not connected to changes in the cell cycle distribution or specific cell loss. Moreover, preliminary data from our laboratory indicate that a similar H1 dephosphorylation pattern was obtained after gamma-irradiation (25 Gy, incubation time of 2−6 h) of Jurkat cells without a major change in the cell cycle distribution (data not shown). We therefore conclude that the previous studies of H1 dephosphorylation were most likely affected by cell cycle alterations caused by the inducing agents, while our results indicate that the detected H1 dephosphorylation is connected to the apoptotic process and/or growth inhibitory signaling preceding changes in the total cell cycle distribution.

The absence of phosphorylated H1 in apoptotic chromatin from serum-deprived PC12 cells has been suggested (*39*). A decrease in the level of phosphate incorporation in histone H1 and dephosphorylation of H1 subtypes was noted after apoptosis induction in NIH 3T3 cells by TNFα or anti-Fas together with cycloheximide (*20*). Also, prolonged treatment with only TNFα resulted in decreased levels of H1 phosphorylation and apoptosis, while cycloheximide treatment alone resulted in the same extent of H1 dephosphorylation that is seen with both substances, but no apoptosis. Interestingly, by caspase inhibition, the H1 dephosphorylation in the TNFα and anti-Fas/cycloheximide systems could be inhibited (*20*). Treatment of Jurkat cells with ionizing radiation also caused a transient dephosphorylation of histone H1 (*16*). On the other hand, when apoptosis was induced in thymocytes by phosphatase inhibitors, the level of histone H1 phosphorylation increased (*21, 22*). Cell cycle disturbances may play a role in H1 phosphorylation changes in these experiments, as well as side effects caused by the apoptosis-inducing agents used, for example, the protein synthesis inhibitor cycloheximide, phosphatase inhibitors, or ionizing radiation. Furthermore, a decreased level of phosphate incorporation may not be equivalent to the actual level of dephosphorylation of H1 histones. We here show that after induction of apoptosis by anti-Fas, where the cell cycle was virtually unaffected, the H1 phosphorylation pattern remained approximately unchanged.

In conclusion, following induction of apoptosis with anti-Fas, the histone H1 phosphorylation pattern remained unchanged, as did cell cycle distribution, despite a large fraction of apoptotic cells. This result indicates that in Jurkat cells, histone H1 maintains a high degree of phosphorylation in the early phase of anti-Fas-induced apoptosis. On the other hand, after camptothecin treatment, histone H1 became rapidly and extensively dephosphorylated. We conclude that histone H1 dephosphorylation is not a general feature in apoptosis but may be coupled to apoptosis by the intrinsic pathway or to concomitant growth inhibitory signaling.

ACKNOWLEDGMENT

We thank Dr. Henrik Gréen for expert help with the flow cytometric analyses.

SUPPORTING INFORMATION AVAILABLE

HPCE separation of H1 histones from Jurkat cells before RPC fractionation overlaid with H1.5 histones from RPC fraction 1 (Figure S1) and HPCE separation of H1 histones from Jurkat cells mixed with purified H1 fractions (Figure S2). This material is available free of charge via the Internet at http://pubs.acs.org.

REFERENCES

1. Thomas, J. O. (1999) Histone H1: Location and role. *Curr. Opin. Cell Biol. 11*, 312–317.
2. Khochbin, S. (2001) Histone H1 diversity: Bridging regulatory signals to linker histone function. *Gene 271*, 1–12.
3. Ponte, I., Vidal-Taboada, J. M., and Suau, P. (1998) Evolution of the vertebrate H1 histone class: Evidence for the functional differentiation of the subtypes. *Mol. Biol. Evol. 15*, 702–708.
4. Fan, Y., Sirotkin, A., Russell, R. G., Ayala, J., and Skoultchi, A. I. (2001) Individual somatic H1 subtypes are dispensable for mouse development even in mice lacking the H1(0) replacement subtype. *Mol. Cell. Biol. 21*, 7933–7943.
5. Parseghian, M. H., and Hamkalo, B. A. (2001) A compendium of the histone H1 family of somatic subtypes: An elusive cast of characters and their characteristics. *Biochem. Cell Biol. 79*, 289–304.
6. Sarg, B., Helliger, W., Talasz, H., Forg, B., and Lindner, H. H. (2006) Histone H1 phosphorylation occurs site-specifically during interphase and mitosis: Identification of a novel phosphorylation site on histone H1. *J. Biol. Chem. 281*, 6573–6580.
7. Bustin, M., Catez, F., and Lim, J. H. (2005) The dynamics of histone H1 function in chromatin. *Mol. Cell 17*, 617–620.
8. Dou, Y., Bowen, J., Liu, Y., and Gorovsky, M. A. (2002) Phosphorylation and an ATP-dependent process increase the dynamic exchange of H1 in chromatin. *J. Cell Biol. 158*, 1161–1170.
9. Contreras, A., Hale, T. K., Stenoien, D. L., Rosen, J. M., Mancini, M. A., and Herrera, R. E. (2003) The dynamic mobility of histone H1 is regulated by cyclin/CDK phosphorylation. *Mol. Cell. Biol. 23*, 8626–8636.
10. Krammer, P. H. (2000) CD95's deadly mission in the immune system. *Nature 407*, 789–795.
11. Khosravi-Far, R., and Esposti, M. D. (2004) Death receptor signals to mitochondria. *Cancer Biol. Ther. 3*, 1051–1057.
12. Hengartner, M. O. (2000) The biochemistry of apoptosis. *Nature 407*, 770–776.
13. Widlak, P., Li, P., Wang, X., and Garrard, W. T. (2000) Cleavage preferences of the apoptotic endonuclease DFF40 (caspase- activated DNase or nuclease) on naked DNA and chromatin substrates. *J. Biol. Chem. 275*, 8226–8232.
14. Widlak, P., Kalinowska, M., Parseghian, M. H., Lu, X., Hansen, J. C., and Garrard, W. T. (2005) The histone H1 C-terminal domain binds to the apoptotic nuclease, DNA fragmentation factor (DFF40/CAD) and stimulates DNA cleavage. *Biochemistry 44*, 7871–7878.
15. Konishi, A., Shimizu, S., Hirota, J., Takao, T., Fan, Y., Matsuoka, Y., Zhang, L., Yoneda, Y., Fujii, Y., Skoultchi, A. I., and Tsujimoto, Y. (2003) Involvement of histone H1.2 in apoptosis induced by DNA double-strand breaks. *Cell 114*, 673–688.

16. Guo, C. Y., Mizzen, C., Wang, Y., and Larner, J. M. (2000) Histone H1 and H3 dephosphorylation are differentially regulated by radiation-induced signal transduction pathways. *Cancer Res. 60*, 5667–5672.
17. Kratzmeier, M., Albig, W., Hanecke, K., and Doenecke, D. (2000) Rapid dephosphorylation of H1 histones after apoptosis induction. *J. Biol. Chem. 275*, 30478–30486.
18. Happel, N., Sommer, A., Hanecke, K., Albig, W., and Doenecke, D. (2005) Topoisomerase inhibitor induced dephosphorylation of H1 and H3 histones as a consequence of cell cycle arrest. *J. Cell. Biochem. 95*, 1235–1247.
19. Goebel, W., Obermeyer, N., Bleicher, N., Kratzmeier, M., Eibl, H. J., Doenecke, D., and Albig, W. (2007) Apoptotic DNA fragmentation is not related to the phosphorylation state of histone H1. *Biol. Chem. 388*, 197–206.
20. Talasz, H., Helliger, W., Sarg, B., Debbage, P. L., Puschendorf, B., and Lindner, H. (2002) Hyperphosphorylation of histone H2A.X and dephosphorylation of histone H1 subtypes in the course of apoptosis. *Cell Death Differ. 9*, 27–39.
21. Lee, E., Nakatsuma, A., Hiraoka, R., Ishikawa, E., Enomoto, R., and Yamauchi, A. (1999) Involvement of histone phosphorylation in thymocyte apoptosis by protein phosphatase inhibitors. *IUBMB Life 48*, 79–83.
22. Enomoto, R., Koyamazaki, R., Maruta, Y., Tanaka, M., Takuma, K., Mori, K., and Lee, E. (2001) Phosphorylation of histones triggers DNA fragmentation in thymocyte undergoing apoptosis induced by protein phosphatase inhibitors. *Mol. Cell. Biol. Res. Commun. 4*, 276–281.
23. Wu, D., Ingram, A., Lahti, J. H., Mazza, B., Grenet, J., Kapoor, A., Liu, L., Kidd, V. J., and Tang, D. (2002) Apoptotic release of histones from nucleosomes. *J. Biol. Chem. 277*, 12001–12008.
24. Vindelöv, L. L., Christensen, I. J., and Nissen, N. I. (1983) A detergent-trypsin method for the preparation of nuclei for flow cytometric DNA analysis. *Cytometry 3*, 323–327.
25. Lindner, H., Sarg, B., and Helliger, W. (1997) Application of hydrophilic-interaction liquid chromatography to the separation of phosphorylated H1 histones. *J. Chromatogr., A 782*, 55–62.
26. Lindner, H., Helliger, W., Dirschlmayer, A., Talasz, H., Wurm, M., Sarg, B., Jaquemar, M., and Puschendorf, B. (1992) Separation of phosphorylated histone H1 variants by high-performance capillary electrophoresis. *J. Chromatogr. 608*, 211–216.
27. Lindner, H., Wurm, M., Dirschlmayer, A., Sarg, B., and Helliger, W. (1993) Application of high-performance capillary electrophoresis to the analysis of H1 histones. *Electrophoresis 14*, 480–485.
28. Happel, N., Doenecke, D., Sekeri-Pataryas, K. E., and Sourlingas, T. G. (2008) H1 histone subtype constitution and phosphorylation state of the ageing cell system of human peripheral blood lymphocytes. *Exp. Gerontol. 43*, 184–199.
29. Pozarowski, P., Huang, X., Halicka, D. H., Lee, B., Johnson, G., and Darzynkiewicz, Z. (2003) Interactions of fluorochrome-labeled caspase inhibitors with apoptotic cells: A caution in data interpretation. *Cytometry, Part A 55*, 50–60.
30. Hueber, A., Durka, S., and Weller, M. (1998) CD95-mediated apoptosis: No variation in cellular sensitivity during cell cycle progression. *FEBS Lett. 432*, 155–157.
31. Karas, M., Zaks, T. Z., Liu, J. L., and LeRoith, D. (1999) T cell receptor-induced activation and apoptosis in cycling human T cells occur throughout the cell cycle. *Mol. Biol. Cell 10*, 4441–4450.
32. N'Cho, M., and Brahmi, Z. (2001) Evidence that Fas-induced apoptosis leads to S phase arrest. *Hum. Immunol. 62*, 310–319.
33. Bae, Y., and Crispe, I. N. (2001) Differential regulation of cell cycle-related proteins by CD95 engagement in thymocytes and T cell leukemic cell line, Jurkat. *J. Cell. Biochem. 80*, 328–338.
34. Parr, T. B., Hofman, F. M., Kiener, P. A., and Stohl, W. (2001) Cell cycle phase-specific survival of CD95 ligand-challenged Jurkat cells: Upregulation of heat-shock response. *Cell. Immunol. 211*, 21–29.
35. Donahue, C. J., Santoro, M., Hupe, D., Jones, J. M., Pollok, B., Heim, R., and Giegel, D. (2001) Correlating cell cycle with apoptosis in a cell line expressing a tandem green fluorescent protein substrate specific for group II caspases. *Cytometry 45*, 225–234.
36. Pizzolato, J. F., and Saltz, L. B. (2003) The camptothecins. *Lancet 361*, 2235–2242.
37. Li, Q. Y., Zu, Y. G., Shi, R. Z., and Yao, L. P. (2006) Review camptothecin: Current perspectives. *Curr. Med. Chem. 13*, 2021–2039.
38. Johnson, N., Ng, T. T., and Parkin, J. M. (1997) Camptothecin causes cell cycle perturbations within T-lymphoblastoid cells followed by dose dependent induction of apoptosis. *Leuk. Res. 21*, 961–972.
39. Hendzel, M. J., Nishioka, W. K., Raymond, Y., Allis, C. D., Bazett-Jones, D. P., and Th'ng, J. P. (1998) Chromatin condensation is not associated with apoptosis. *J. Biol. Chem. 273*, 24470–24478.

BI702311X